Journal of the Serbian Chemical Society
JSCS-info@shd.org.rs • www.shd.org.rs/JSCS
J. Serb. Chem. Soc. 81 (5) 521–539 (2016)
JSCS–4865
UDC 546.962+547.497.1:544.022:532.14:519.677:535–31
Original scientific paper

Effect of principal and secondary ligands on the electronic structures and spectra of a series of ruthenium(II) complexes

YANLI ZHANG[1], JIEQIONG LI[2] and LI WANG[2]*

[1]*School of Materials and Chemical Engineering, Zhongyuan University of Technology, Zhongyuan 450007, P. R. China and* [2]*Institute of Environmental and Analytical Sciences, College of Chemistry and Chemical Engineering, Henan University, Kaifeng, Henan 475004, P. R. China*

(Received 29 October 2015, revised 15 January, accepted 17 February 2016)

Abstract: A DFT (density functional theory)/TDDFT (time-dependent density functional theory) investigation was performed to study the ground-state geometries, electronic structures and absorption spectra of twelve ruthenium(II) thiosemicarbazone complexes, [Ru(CO)(X)(L^n)], where L^n are derivatives of a dibasic tetradentate Schiff-base ligands and X stands for $AsPh_3$/PPh_3/Py. The ground-state geometries were optimized at the B3LYP/6-31G(d)-LANL2DZ level, and the spectra were simulated by means of the TD-B3LYP/6-31G(d)--LANL2DZ method based on the optimized geometries. The influence of the principal and secondary ligands (L^n and X) on the transition characters and absorption peak positions was evaluated.

Keywords: spectroscopy; Ru(II) complexes; thiosemicarbazone; tetradentate.

INTRODUCTION

Thiosemicarbazones have received continuous great attention primarily because of their bioinorganic relevance[1] in general and their biological activities including antibacterial, antiviral, antimalarial and anticancer activities.[2–4] On the other hand, thiosemicarbazones have emerged as an important class of sulfur donor ligands for transition metal ions because of their mixed hard–soft donor character and versatile coordination behavior. In the past few years, most studies were concerned with iron, copper, nickel, cobalt, zinc, mercury and ruthenium complexes.[5–7] Schiff bases offer opportunities for inducing substrate chirality, tuning metal-centered electronic factors, enhancing solubility and stability, and behaving as either homogenous or heterogeneous catalysts.[8–10] Except for these common properties, Ru(II) complexes are a fascinating class of molecules for application as light emitting devices (LED).[11] Ruthenium(II) compounds display

* Corresponding author. E-mail: chemwangl@henu.edu.cn
doi: 10.2298/JSC151029031Z

long lived luminescence and extreme photostability.[12] Although there is a wealth of information available on the ruthenium bi- or polypyridyl complexes, the luminescent chemistry of ruthenium(II) complexes containing Schiff bases has not been well developed.

Recently, many ruthenium complexes with Schiff bases have been synthesized by several groups,[13–16] while a series of ruthenium(II) thiosemicarbazone complexes containing triphenylphosphine/triphenylarsine/pyridine as co--ligands, synthesized by Jayabalakrishnan and co-workers,[17] aroused our interest. However, neither structural information nor detailed transition information of the spectrum were reported in their work, which is a common perplexity for almost all experimentalists. There is no doubt that quantum chemistry is a promising tool to testify the experimental result and/or provide instructive clues to discover new properties and compounds.

In this work, a series of $Ru(CO)(X)(L^n)$ complexes (see Fig. 1) were theoretically investigated, where L^n = derivatives of a dibasic tetradentate Schiff-base ligand (principal ligand), X = $AsPh_3$/PPh_3/pyridine (secondary ligand). Totally, twelve Ru(II) complexes were studied, *i.e.*, $RuCO(AsPh_3)L^1$ (**A**), $RuCO(PPh_3)L^1$

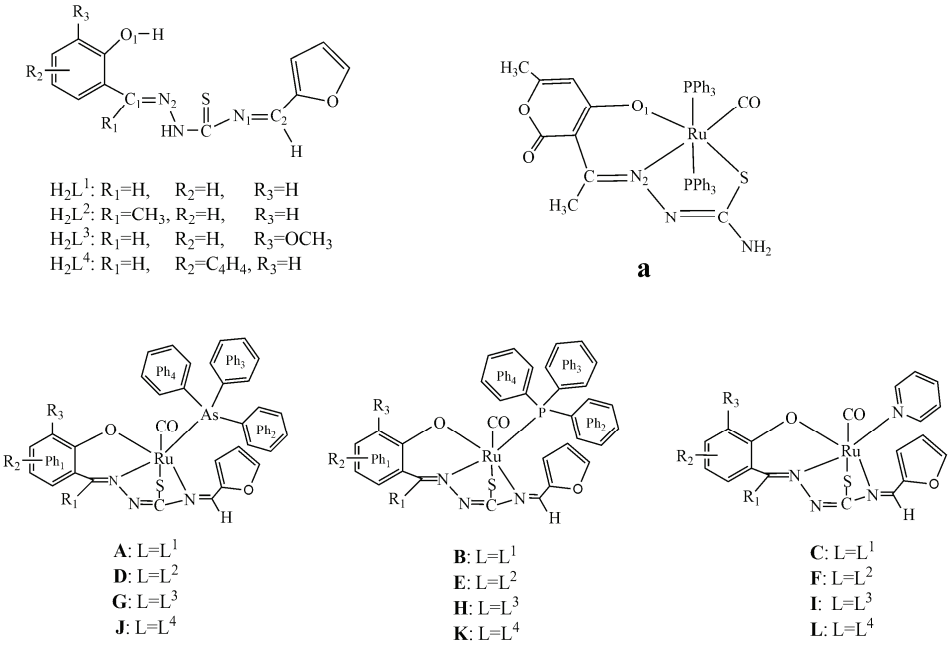

Fig. 1. Schematic structures of ligands H_2L^1, H_2L^2, H_2L^3 and H_2L^4, and the corresponding complexes $RuCO(AsPh_3)L^1$ (**A**), $RuCO(PPh_3)L^1$ (**B**), $RuCO(Py)L^1$ (**C**), $RuCO(AsPh_3)L^2$ (**D**), $RuCO(PPh_3)L^2$ (**E**), $RuCO(Py)L^2$ (**F**), $RuCO(AsPh_3)L^3$ (**G**), $RuCO(PPh_3)L^3$ (**H**), $RuCO(Py)L^3$ (**I**), $RuCO(AsPh_3)L^4$ (**J**), $RuCO(PPh_3)L^4$ (**K**), and $RuCO(Py)L^4$ (**L**) with the experimental[14] structure of complex **a**.

(**B**), RuCO(Py)L^1 (**C**), RuCO($AsPh_3$)L^2 (**D**), RuCO(PPh_3)L^2 (**E**), RuCO(Py)L^2 (**F**), RuCO($AsPh_3$)L^3 (**G**), RuCO(PPh_3)L^3 (**H**), RuCO(Py)L^3 (**I**), RuCO($AsPh_3$)L^4 (**J**), RuCO(PPh_3)L^4 (**K**) and RuCO(Py)L^4 (**L**). The geometric and electronic structures were calculated by the B3LYP method. Furthermore, the spectra were simulated by the TD-B3LYP method based on the optimized geometries. The general goals of this work were to understand in depth the spectroscopic properties by detailed electronic transition and orbital analysis and to cast light on the effect of the principal and secondary ligands on the spectroscopic properties.

COMPUTATIONAL DETAILS

All calculations involved in this study were completed by the Gaussian 09[18] program package. Geometry optimizations were performed without any symmetry constraints by means of the B3LYP (Becke's three-parameter nonlocal-exchange functional[19] with the non--local correlation of the Lee–Yang–Parr) method.[20,21] The vibrational frequencies were calculated at the same level to characterize the nature of the stationary point. Some selected frequencies are listed in Table S-I of the Supplementary material to this paper along with the experimental values. The deviations between experimental and theoretical values were less than 0.06 %, indicating the accuracy of the employed DFT method. Moreover, two other DFT methods, PBE1PBE (the GGA exchange-correlation functionals of Perdew, Burke and Ernzerhof)[22] and M06[23] were employed to optimize the structures of complexes **A**, **B** and **C**. A mixed basis set, *i.e.*, the 6-31G(d) basis set[24,25] for C, H, O, N, S and As atoms, and the "double-ζ" quality basis set LANL2DZ associated with quasi-relativistic pseudo-potentials proposed by Hay and Wadt[26-28] with 16 valence electrons for the Ru(II) atom were adopted.

Based on the optimized geometries, the absorption spectra of all complexes were examined by TDDFT[29-31] in dichloromethane solvent with the same mixed basis set. The solvent effect was considered by means of the polarized continuum model (PCM)[32,33] algorithm.

RESULTS AND DISCUSSION

Geometry of structures

The schematic structures of the four ligands (H_2L^1, H_2L^2, H_2L^3 and H_2L^4) and the corresponding twelve ruthenium(II) complexes [Ru(CO)(X)(L^n)] (where X is $AsPh_3$/PPh_3/Py and L^n are derivatives of dibasic tetradentate Schiff-base ligand) are shown in Fig. 1 together with the labeling of the phenyl rings and key atoms. Due to the absence of X-ray diffraction data on single crystals of the twelve investigated complexes, it is difficult to estimate the accuracy of the calculated geometries. Alternatively, the structures of representative complexes (**A**, **B** and **C**) were optimized by three DFT methods, *i.e.*, B3LYP, PBE1PBE and M06, to compare them with each other. Moreover, the geometry of complex **B** was compared with the experimental data[14] for complex **a** with a similar ligand and coordination environment (the structure is also shown in Fig. 1). The corresponding results are listed in Table S-II of the Supplementary material. After comparison, the B3LYP method was finally employed to optimize the geometries of the other complexes.

The optimized structures of the twelve ruthenium(II) complexes containing tetradentate Schiff bases determined at the B3LYP level are depicted in Figs. S-1 and S-2 of the Supplementary material. Their key bond lengths and angles are tabulated in Tables I–III. These complexes are distinguished with each other according to the two ligands, X and L^n, where L^n is considered as the primary ligand and X as the secondary ligand. From the geometric parameters, the following information was obtained: 1) all the Schiff-base complexes present a distorted octahedral environment around the ruthenium(II), which is similar to that of other ruthenium(II) complexes;[1,14,34] 2) the thiosemicarbazone ligand coordinates to the metal center with C, N, O and S, forming a four-membered, a five--membered, and a six-membered metallacycle; 3) neither the first nor the second ligand greatly affects the key bond lengths and angles.

TABLE I. Calculated bond lengths and angles for $RuCO(AsPh_3)L^1$ (**A**), $RuCO(AsPh_3)L^2$ (**D**), $RuCO(AsPh_3)L^3$ (**G**) and $RuCO(AsPh_3)L^4$ (**J**) obtained by the B3LYP/6-31G(d)-LANL2DZ method

Bond	$RuCO(AsPh_3)L^1$	$RuCO(AsPh_3)L^2$	$RuCO(AsPh_3)L^3$	$RuCO(AsPh_3)L^4$
		Bond length, Å		
Ru–As	2.49	2.49	2.49	2.49
Ru–C	1.90	1.90	1.90	1.90
$Ru–N_1$	2.14	2.13	2.14	2.14
$Ru–N_2$	2.05	2.06	2.05	2.06
$Ru–O_1$	2.11	2.10	2.11	2.11
Ru–S	2.51	2.50	2.51	2.52
		Bond angle, °		
As–Ru–C	91.65	91.76	91.55	91.56
$As–Ru–N_1$	167.38	167.61	167.51	167.85
$As–Ru–N_2$	98.36	98.02	98.30	98.49
$C–Ru–N_1$	98.35	98.33	98.47	98.47
$C–Ru–N_2$	169.16	169.53	169.40	169.21
$N_1–Ru–N_2$	71.19	71.51	71.26	71.09
$O_1–Ru–S$	154.42	153.99	154.00	153.92

TABLE II. Calculated bond lengths and angles for $RuCO(PPh_3)L^1$ (**B**), $RuCO(PPh_3)L^2$ (**E**), $RuCO(PPh_3)L^3$ (**H**) and $RuCO(PPh_3)L^4$ (**K**) obtained by the B3LYP/6-31G(d)-LANL2DZ method

Bond	$RuCO(PPh_3)L^1$	$RuCO(PPh_3)L^2$	$RuCO(PPh_3)L^3$	$RuCO(PPh_3)L^4$
		Bond lengths, Å		
Ru–P	2.39	2.39	2.39	2.39
Ru–C	1.90	1.90	1.90	1.90
$Ru–N_1$	2.16	2.15	2.15	2.16
$Ru–N_2$	2.06	2.07	2.05	2.06
$Ru–O_1$	2.11	2.10	2.11	2.11
Ru–S	2.51	2.50	2.51	2.51

TABLE II. Continued

Bond	$RuCO(PPh_3)L^1$	$RuCO(PPh_3)L^2$	$RuCO(PPh_3)L^3$	$RuCO(PPh_3)L^4$
		Bond angles, °		
P–Ru–C	92.41	92.20	92.15	92.11
P–Ru–N_1	166.93	167.29	167.15	167.20
P–Ru–N_2	98.52	98.75	98.72	99.02
C–Ru–N_1	97.84	97.59	97.86	97.93
C–Ru–N_2	168.31	168.44	168.47	168.20
N_1–Ru–N_2	70.76	71.05	70.84	70.51
O_1–Ru–S	153.91	153.71	153.57	153.60

TABLE III. Calculated bond lengths and angles for $RuCO(Py)L^1$ (**C**), $RuCO(Py)L^2$ (**F**), $RuCO(Py)L^3$ (**I**) and $RuCO(Py)L^4$ (**L**) obtained by the by B3LYP/6-31G(d)-LANL2DZ method

Bond	$RuCO(Py)L^1$	$RuCO(Py)L^2$	$RuCO(Py)L^3$	$RuCO(Py)L^4$
		Bond lengths, Å		
Ru–N	2.17	2.17	2.17	2.17
Ru–C	1.91	1.90	1.91	1.90
Ru–N_1	2.10	2.10	2.10	2.10
Ru–N_2	2.05	2.06	2.05	2.05
Ru–O_1	2.10	2.08	2.09	2.09
Ru–S	2.53	2.52	2.53	2.53
		Bond angles, °		
N–Ru–C	93.06	92.88	92.80	92.88
N–Ru–N_1	166.87	167.25	167.30	167.20
N–Ru–N_2	95.56	95.58	95.92	96.02
C–Ru–N_1	98.90	98.83	98.81	98.83
C–Ru–N_2	170.63	170.82	170.61	170.44
N_1–Ru–N_2	72.18	72.44	72.21	72.01
O_1–Ru–S	155.56	155.32	155.24	155.16

Molecular orbitals

The optical and other chemical properties are governed by the ground-state electronic structure, especially for the frontier orbitals (HOMO – the highest occupied molecular orbital and LUMO – the lowest unoccupied molecular orbital). Thus, elucidating the HOMO and LUMO distributions, energy levels, energy gaps, and other detailed electronic structure information is helpful to cast light on the absorption spectra intrinsically. The orbital compositions for several selected frontier orbitals (including four highest HOMOs and three lowest LUMOs) of complexes **A**–**L** are illustrated in Tables S-III–S-XIV of the Supporting material. The plots of selected molecular orbitals involved in the key absorptions (energy levels, and energy gaps of twelve complexes are plotted in Figs. 2–5).

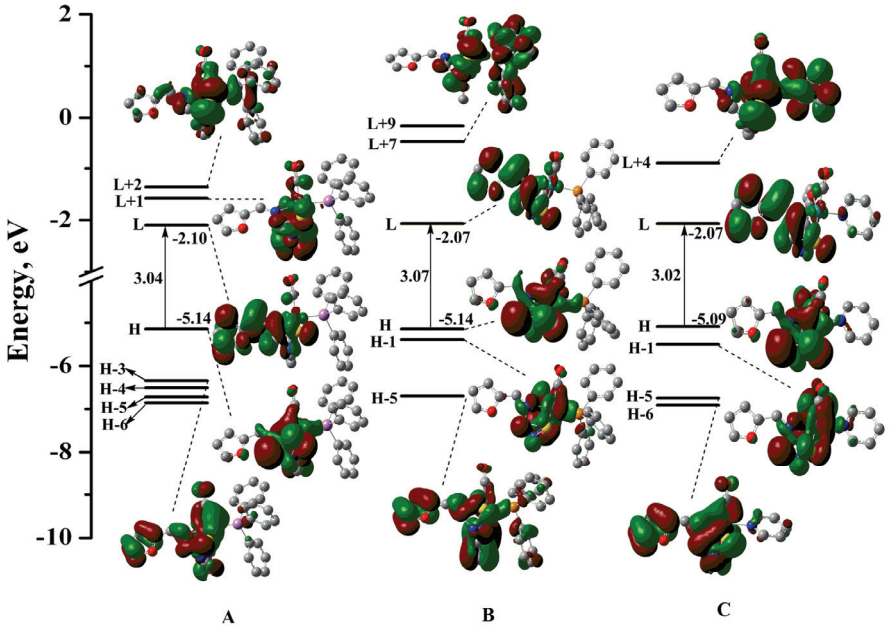

Fig. 2. Presentation of the energy levels, energy gaps, and counter plots of selected molecular orbitals involved in the absorption spectra for complexes $RuCO(AsPh_3)L^1$ (**A**), $RuCO(PPh_3)L^1$ (**B**) and $RuCO(Py)L^1$ (**C**).

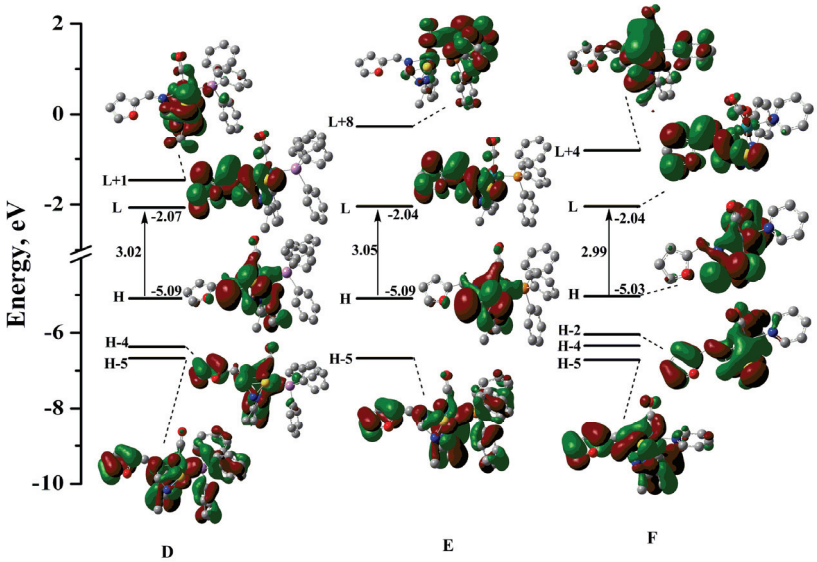

Fig. 3. Presentation of the energy levels, energy gaps, and counter plots of selected molecular orbitals involved in the absorption spectra for complexes $RuCO(AsPh_3)L^2$ (**D**), $RuCO(PPh_3)L^2$ (**E**) and $RuCO(Py)L^2$ (**F**).

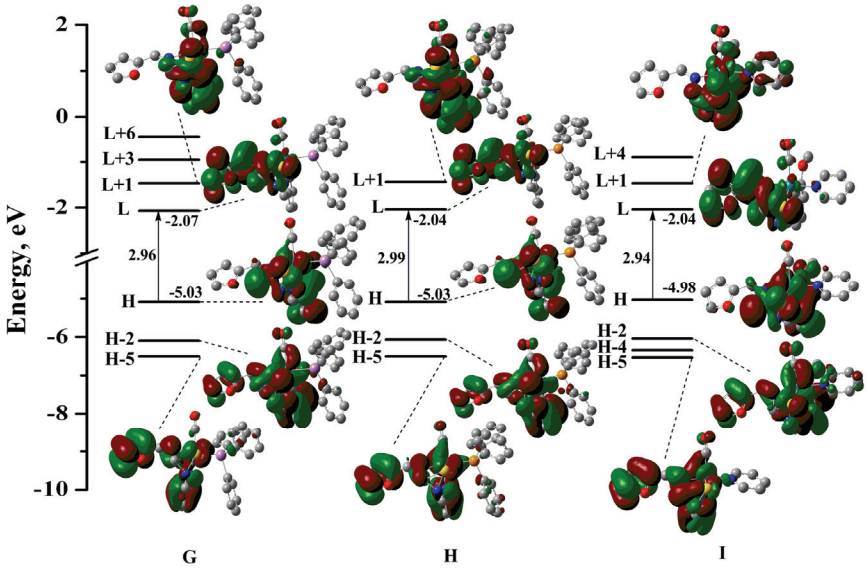

Fig. 4. Presentation of the energy levels, energy gaps, and counter plots of selected molecular orbitals involved in the absorption spectra for complexes $RuCO(AsPh_3)L^3$ (**G**), $RuCO(PPh_3)L^3$ (**H**), and $RuCO(Py)L^3$ (**I**).

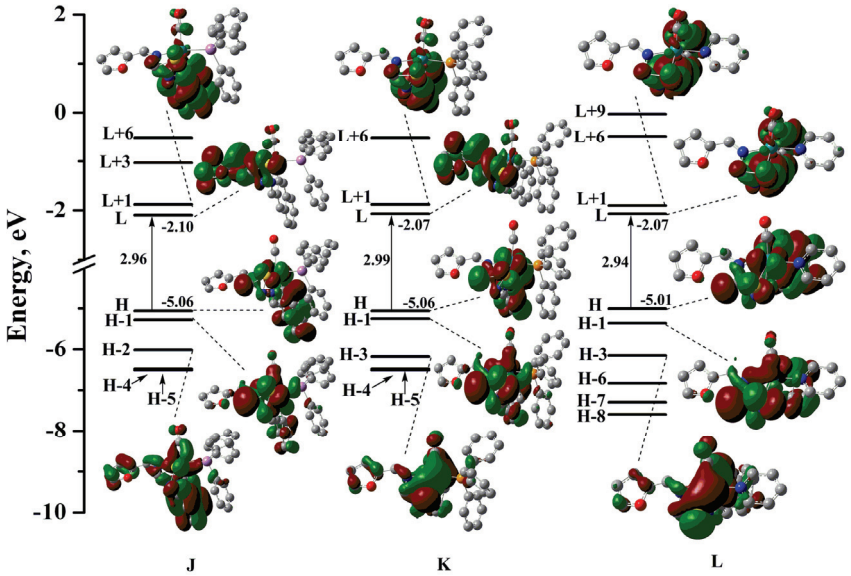

Fig. 5. Presentation of the energy levels, energy gaps, and counter plots of selected molecular orbitals involved in the absorption spectra for complexes $RuCO(AsPh_3)L^4$ (**J**), $RuCO(PPh_3)L^4$ (**K**), and $RuCO(Py)L^4$ (**L**).

When the principal ligand (L^n) is fixed, the investigated complexes are categorized into four groups, *i.e.*, (I) **A**, **B**, and **C** ($L^n = L^1$), (II) **D**, **E**, and **F** ($L^n = = L^2$), (III) **G**, **H**, and **I** ($L^n = L^3$), and (IV) **J**, **K**, and **L** ($L^n = L^4$). When the secondary ligand (X) is fixed, they are classified into three groups, *i.e.*, *i*) **A**, **D**, **G**, and **J** (X = $AsPh_3$), *ii*) **B**, **E**, **H**, and **K** (X = PPh_3), and *iii*) **C**, **F**, **I**, and **L** (X = = Py). For complex **A**, the HOMO (H), at –5.14 eV, is mainly distributed over the d-orbital of Ru, the p-orbitals of C, and the S atoms in part a, and Ph_1(phenyl), as well as a negligible contribution from the O_1 atom. H-1, H-2, and H-3 are separated by 0.28, 1.01 and 1.20 eV from the HOMO with similar distributions to that of the HOMO except that the compositions of different parts change a little. The contribution of the d-orbital of Ru increases from H-1 to H-3, while the composition of Ph_1 decreases. Furan (Fu) becomes more important in the H-2 and H-3 orbitals and the O_1 atom plays a more important role for the H-1 and H-3 orbitals. The orbital compositions of **B** and **C** are very similar to those for **A**. The LUMOs of **A**–**C** are dominantly resided on the furan, C_2 atom, and part a. On the contrary, the electronic distributions on the Ru atom and the Ph_1 ring are decreased. The contribution of an ancillary ligand is almost negligible except for the LUMO+2 of complex **C**, which is predominantly localized on the Py (pyridine) moiety. In summary, the –$AsPh_3$ and –PPh_3 moieties as the secondary ligand have a smaller effect on the electron density than the pyridine does. The other three groups (II), (III), and (IV) with similar properties will not be discussed again.

Next, the influence of the primary ligand on the electron distribution will be discussed. As compared with complex **A**, the H atom replaced by a –CH_3 group (complex **D**) did not make a great change in the frontier molecular orbitals (FMOs), while the contribution from the ending moiety of complex **G** and complex **J** increased them, especially the HOMO. The addition of an electron-donating group on the C_1 atom had almost no influence. However, the electron density would be increased by the addition of an electron-donating group on the phenyl ring (complex **G**) or increasing the π-conjugation by variation of the phenyl group to a Naph (naphthyl) group (complex **J**). The other two groups *ii*) and *iii*) had a similar behavior.

Except for the electron distribution, the influence of different ligands on the energy gap is also worthy of attention. When the principal ligand (L^n) was the same, the H–L energy gaps of the group *i*) increased in the following sequence: **C**→**A**→**B**, *i.e.*, X = Py< X = $AsPh_3$ < X = PPh_3. The other three groups also obeyed this sequence. If the secondary ligand was the same, the H–L energy gaps decreased from L^1 to L^4. However, the largest deviation in the same group was only 0.06 eV, which is too small to distinguish them. Thus, the influence of the principal and the secondary ligands on the lowest-lying transition will not be clear-cut.

Electronic spectra

The lowest 50 singlet–singlet excitations based on the optimized geometries in the gas phase were calculated in CH_2Cl_2 solvent using the PCM model to gain insight into the nature of the absorption state. In addition to the geometric structure, the absorption spectrum is also related to the employed functional. Thus, the absorption spectra of complexes **A**, **B**, and **C** were theoretically simulated by the three above-mentioned functionals based on their corresponding optimized geometries. The fitted Gaussian type absorption curves obtained from the different methods are plotted in Fig. S-3 of the Supplementary material with a full width at half maximum (FWHM) of 0.4 eV. As shown in Fig. S-3, the position and shape of the absorption spectra obtained by the PBE1PBE and M06 methods were similar to each other, but far removed from the B3LYP results and the experimental data. Moreover, considering that it is advantageous to obtain different molecular features, ranging from geometries to vertical excitation energies, using the same method and almost the same basis set, as indicated by Perdew *et al.*,[22] the TD-B3LYP/6-31G(d)-LANL2DZ//B3LYP/6-31G(d)--LANL2DZ level was adopted to simulate the absorption features of the other complexes.

Some leading absorptions along with the oscillator strengths, configuration interaction (*CI*) coefficient, assignments as well as the experimental values for complexes **A**–**L** are summarized in Tables IV–VII. In addition, the absorption spectra of the twelve ruthenium(II) complexes in dichloromethane solvent simulated by means of the TD-B3LYP method are shown graphically in Figs. 6–9 (the primary ligand was fixed) and Figs. S-4–S-6 of the Supplementary material (the second ligand was fixed), respectively. Since the absorption curves of the complexes in the same group are almost superimposed, the intensity of each complex in every group was shifted by 0.05 as compared with the former ones for clear presentation in Figs. 6–9.

TABLE IV. Calculated absorptions of complexes $RuCO(AsPh_3)L^1$ (**A**), $RuCO(PPh_3)L^1$ (**B**) and $RuCO(Py)L^1$ (**C**) in dichloromethane medium at the TD-B3LYP level, together with the experimental values[17]

Cmpd.	State	λ nm	Oscillator strength	Main configuration	Assignments	$\lambda_{Expt.}$ nm
A	S_1	567	0.0057	H→L (91 %)	$Ph_1/C_a/S_a/Ru \rightarrow Fu/C_2/N_a$ IL/MLCT	
	S_4	444	0.0213	H→L+1 (87 %)	$Ph_1/C_a/S_a/Ru \rightarrow Ph_1/C_1/N_a$ IL/MLCT	450
	S_{14}	331	0.1326	H-4→L (36 %)	$Ph_1/Fu/Ru \rightarrow Fu/C_2/N_a$ IL/MLCT	347
	S_{25}	298	0.1915	H-5→L (25 %)	$Ph_1/Ph_4 \rightarrow Fu/C_2/N_a$ IL/LLCT	

TABLE IV. Continued

Cmpd.	State	λ nm	Oscillator strength	Main configuration	Assignments	$\lambda_{Expt.}$ nm
A	S_{51}	261	0.1393	H-6→L+2 (28 %)	$Ph_2/Ph_3/Ph_4/Ru→S_a/Ru$ LL/LMCT/MC	258
B	S_1	566	0.0059	H→L (93 %)	$C_a/S_a/Ru→Fu/C_2/N_a$ IL/MLCT	
	S_{14}	330	0.0964	H-2→L+1 (27 %)	$Ph_1/Fu/S_a/N_a/Ru→Ph_1/C_1/N_a$ IL/MLCT	355
	S_{24}	301	0.2860	H→L+7 (25 %)	$C_a/S_a/Ru→Ph_2/Ph_3/Ph_4$ LL/MLCT	
	S_{51}	262	0.0719	H-6→L+2 (45 %)	$Ph_2/Ph_3/Ph_4/Ru→S_a/Ru$ LL/MLCT/MC	254
C	S_1	565	0.0085	H→L (92 %)	$Ph/C_a/S_a/Ru→Fu/C_2/N_a$ IL/MLCT	
	S_4	455	0.0229	H→L+1 (90 %)	$Ph/C_a/S_a/Ru→Ph/C_1/N_a$ IL/MLCT	456
	S_{14}	340	0.1064	H-4→L (18 %)	$Ru→Fu/C_2/N_a$ MLCT	362
	S_{28}	293	0.3399	H-5→L (48 %)	$Ph/Fu/N_a/Ru→Fu/C_2/N_a$ IL/MLCT/LC	294
	S_{39}	264	0.0849	H-7→L (83 %)	$Ph/C_1/C_2/Fu/C_a/S_a/N_a/Ru→Fu/C_2/N_a$IL/MLCT/LC	254
	S_{60}	234	0.0807	H-1→L+9 (34 %)	$Ph/O_1/C_a/N_a/Ru→Ph/C_1/O_1$ IL/MLCT	

TABLE V. Calculated absorptions of the complexes $RuCO(AsPh_3)L^2$ (**D**), $RuCO(PPh_3)L^2$ (**E**) and $RuCO(Py)L^2$ (**F**) in dichloromethane medium at the TD-B3LYP level, together with the experimental values[17]

Cmpd.	State	λ nm	Oscillator strength	Main configuration	Assignments	$\lambda_{Expt.}$ nm
D	S_1	574	0.0052	H→L (91 %)	$Ph_1/C_a/S_a/Ru→Fu/C_2/N_a$ IL/MLCT	
	S_{13}	334	0.1727	H-4→L (43 %)	$Ph_1/Fu/Ru→Fu/C_2/N_a$ IL/MLCT	342
	S_{24}	299	0.3908	H-5→L (42 %)	$Ph_1/Fu→Fu/C_2/N_a$ ILCT/LC	314
	S_{49}	263	0.0967	H-6→L+1 (35 %)	$Ph_2/Ru→Ph_1/C_1/S_a/N_a$ LL/MLCT	
	S_{61}	249	0.0452	H→L+14 (22 %)	$Ph_1/C_a/S_a/Ru→Ph_1/O_1/Ru$ IL/MLCT/MC	252
E	S_1	573	0.0049	H→L (93 %)	$C_a/S_a/Ru→Fu/C_2/N_a$ IL/MLCT	
	S_{15}	331	0.0725	H-4→L+2 (16 %)	$Ru→S_a/N_a/Ru$ MLCT/MC	356
	S_{24}	300	0.2131	H-5→L (27 %)	$Ph_1/Fu/Ph_4→Fu/C_2/N_a$ IL/LLCT	

TABLE V. Continued

Cmpd.	State	λ nm	Oscillator strength	Main configuration	Assignments	$\lambda_{Expt.}$ nm
E	S_{43}	270	0.0660	H-12→L (33 %)	$Ph_1/C_a/S_a/N_a/Fu/Ru→Fu/C_2/N_a$ LL/MLCT	
	S_{66}	246	0.0340	H-1→L+13 (15 %)	$Ph_1/O_1/N_a/Ru→Ph_1/Fu/O_1/C_a/S_a$ IL/MLCT	252
F	S_1	574	0.0082	H→L (92 %)	$Ph/C_a/S_a/O_1/Ru→Fu/C_2/N_a$ IL/MLCT	
	S_{12}	346	0.1362	H-4→L (39 %)	$Ph/Ru→Fu/C_2/N_a$ IL/MLCT	357
	S_{27}	294	0.2601	H-5→L (36 %)	$Ph/Fu/N_a/Ru→Fu/C_2/N_a$ IL/MLCT/LC	301
	S_{42}	259	0.0714	H-3→L+5 (21 %)	$Ph/O_1/Ru→Py$ LL/MLCT	254
	S_{65}	231	0.0767	H→L+11 (14 %)	$Ph/C_a/S_a/O_1/Ru→Py/C_2$ IL/LL/MLCT	

TABLE VI. Calculated absorptions of the complexes $RuCO(AsPh_3)L^3$ (**G**), $RuCO(PPh_3)L^3$ (**H**) and $RuCO(Py)L^3$ (**I**) in dichloromethane medium at the TD-B3LYP level, together with the experimental values[17]

Cmpd.	State	λ nm	Oscillator strength	Main configuration	Assignments	$\lambda_{Expt.}$ nm
G	S_1	571	0.0054	H→L (66 %)	$Ph_1/C_a/O_1/Ru→Fu/C_2/N_a$ IL/MLCT	
	S_4	443	0.0232	H→L+1 (67 %)	$Ph_1/C_a/O_1/Ru→Ph_1/C_1/N_a$ IL/MLCT	442
	S_{10}	362	0.0762	H-2→L (27 %)	$Ph_1/Fu/N_a/Ru→Fu/C_2/N_a$ IL/MLCT	349
	S_{21}	310	0.2877	H-5→L (27 %)	$Ph_1/Fu/N_a→Fu/C_2/N_a$ IL/LLCT/LC	301
	S_{47}	268	0.0755	H-13→L (81 %)	$Fu/C_a/N_a/S_a/Ru→Fu/C_2/N_a$ IL/MLCT	
	S_{74}	243	0.0850	H→L+14 (24 %)	$Ph_1/C_a/O_1/Ru→Ph_1/O_1$ IL/MLCT	253
H	S_1	569	0.0052	H→L (63 %)	$Ph_1/O_1/C_a/Ru→Fu/C_2/N_a$ IL/MLCT	
	S_{10}	362	0.0871	H-2→L (43 %)	$Ph_1/Fu/S_a/N_a/Ru→Fu/C_2/N_a$ IL/MLCT	363
	S_{22}	310	0.2781	H-5→L (26 %)	$Ph_1/Fu/N_a/Ru→Fu/C_2/N_a$ IL/MLCT	294
	S_{43}	272	0.0514	H-1→L+10 (45 %)	$Ph_1/C_a/S_a/N_a→Ph_2/Ph_3/CO$ IL/LLCT	
	S_{77}	242	0.1212	H→L+14 (21 %)	$Ph_1/O_1/C_a/Ru→$ $→Ph_1/O_1/N_a/C_a/Fu/CO/Ru$ IL/LL/MLCT/MC	252

TABLE VI. Continued

Cmpd.	State	λ nm	Oscillator strength	Main configuration	Assignments	$\lambda_{Expt.}$ nm
I	S_1	573	0.0089	H→L (85 %)	$Ph/C_a/O_1/Ru \rightarrow Fu/C_2/N_a$ IL/MLCT	
	S_4	456	0.0213	H→L+1 (85 %)	$Ph/C_a/O_1/Ru \rightarrow Ph/C_1/N_a$ IL/MLCT	456
	S_{10}	369	0.1326	H-2→L (81 %)	$Ph/Fu/N_a/Ru \rightarrow Fu/C_2/N_a$ IL/MLCT	362
	S_{23}	304	0.3204	H-5→L (19 %)	$Ph/Fu/N_a/Ru \rightarrow Fu/C_2/N_a$ IL/MLCT	293
	S_{38}	268	0.1354	H-7→L (69 %)	$Ph/N_a \rightarrow Fu/C_2/N_a$ ILCT	254
	S_{65}	230	0.0970	H-1→L+10 (29 %)	$Ph/C_a/S_a/N_a \rightarrow Ph/O_1$ ILCT	

TABLE VII. Calculated absorptions of the complexes $RuCO(AsPh3)L^4$ (**J**), $RuCO(PPh3)L^4$ (**K**) and $RuCO(Py)L^4$ (**L**) in dichloromethane medium at the TD-B3LYP level, together with experimental values[17]

Cmpd.	State	λ nm	Oscillator strength	Main configuration	Assignments	$\lambda_{Expt.}$ nm
J	S_1	564	0.0050	H→L (49 %)	$Naph/O_1/Ru \rightarrow Fu/C_2/N_a$ IL/MLCT	
	S_4	493	0.0237	H→L+1 (82 %)	$Naph/O_1/Ru \rightarrow Naph/C_1/N_a$ IL/MLCT/LC	460
	S_9	370	0.0959	H-2→L (58 %)	$Naph/N_a/Ru \rightarrow Fu/C_2/N_a$ IL/MLCT	373
	S_{14}	345	0.2349	H-2→L+1 (57 %)	$Naph/N_a/Ru \rightarrow Naph/C_1/N_a$ IL/MLCT/LC	334
	S_{21}	314	0.2479	H-4→L (50 %)	$Naph/N_a/Fu/Ru \rightarrow Fu/C_2/N_a$ IL/MLCT/LC	
	S_{58}	262	0.0830	H-6→L+2 (20 %)	$Ph_2 \rightarrow S_a/Ru$ LL/LMCT	
	S_{80}	245	0.0622	H-14→L (50 %)	$Ph_2/Ph_3/Ph_4/Ru \rightarrow Fu/C_2/N_a$ LL/MLCT	254
K	S_1	561	0.0058	H-1→L (52 %)	$Naph/C_a/S_a/N_a \rightarrow Fu/C_2/N_a$ ILCT	
	S_4	491	0.0190	H→L+1 (67 %)	$Naph/O_1/Ru \rightarrow Naph/C_1/N_a$ IL/MLCT/LC	484
	S_9	370	0.0640	H-2→L (56%)	$Naph/N_a/Ru \rightarrow Fu/C_2/N_a$ IL/MLCT	382
	S_{14}	344	0.2697	H-2→L+1 (62 %)	$Naph/N_a/Ru \rightarrow Naph/C_1/N_a$ IL/MLCT/LC	
	S_{33}	293	0.1945	H-1→L+6 (33 %)	$Naph/C_a/S_a/N_a \rightarrow Naph/Ph_2$ IL/LLCT	294

TABLE VII. Continued

Cmpd.	State	λ nm	Oscillator strength	Main configuration	Assignments	$\lambda_{Expt.}$ nm
	S_{48}	272	0.1008	H-1→L+11 (43 %)	Naph/C_a/S_a/N_a→ Naph/O_1/C_a/S_a/N_a/CO/Ph_2/Ph_4/Ru IL/LL/LMCT	
	S_{77}	247	0.0690	H-3→L+7 (12 %)	O_1/S_a/Ru→Ph_2 LL/MLCT	253
L	S_1	566	0.0088	H→L (77 %)	Naph/O_1/Ru→Fu/C_2/N_a IL/MLCT	
	S_{10}	369	0.1041	H-3→L (65 %)	O1/Sa/Ru→Fu/C2/Na IL/MLCT	373
	S_{24}	308	0.3458	H-6→L (21 %)	Fu/Ru→Fu/C_2/N_a IL/MLCT/LC	
	S_{34}	285	0.1584	H-1→L+6 (83 %)	Naph/C_a/S_a→Naph/C_1 ILCT	286
	S_{62}	243	0.1453	H-8→L+1 (32 %)	Py→Naph/C_1/N_a LLCT	253

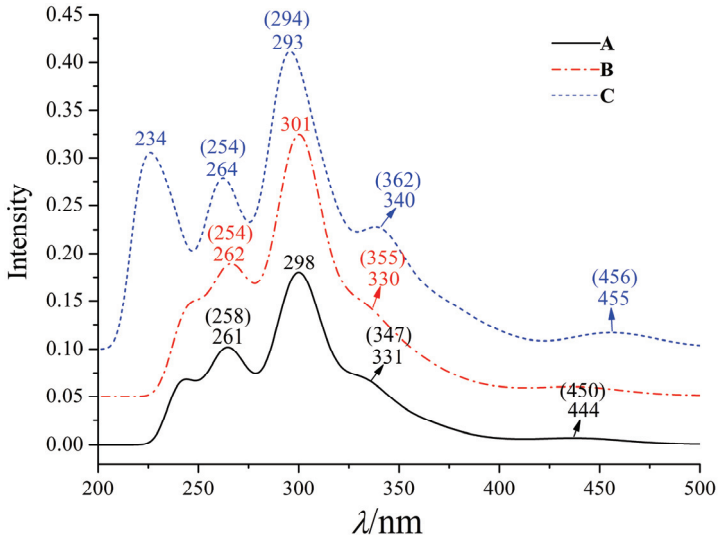

Fig. 6. Simulated absorption spectra (with Intensity as absorbance, *A*) in dichloromethane of complexes RuCO($AsPh_3$)L^1 (**A**), RuCO(PPh_3)L^1 (**B**), and RuCO(Py)L^1 (**C**) from the TD-B3LYP(PCM) calculations, together with the experimental values in parentheses.

The absorption spectrum of complex **A** contains one intense absorption peak centered at 298 nm, two other moderate absorption peaks at 261 and 331 nm and one weak absorption peak at 444 nm. In terms of the peak positions, the theoretical absorptions at 261, 331 and 444 nm are respectively correlated with the experimental peaks at 258, 347 and 450 nm, which have smaller deviations. Moreover, the calculated oscillator strength of the absorption band at 261 nm is

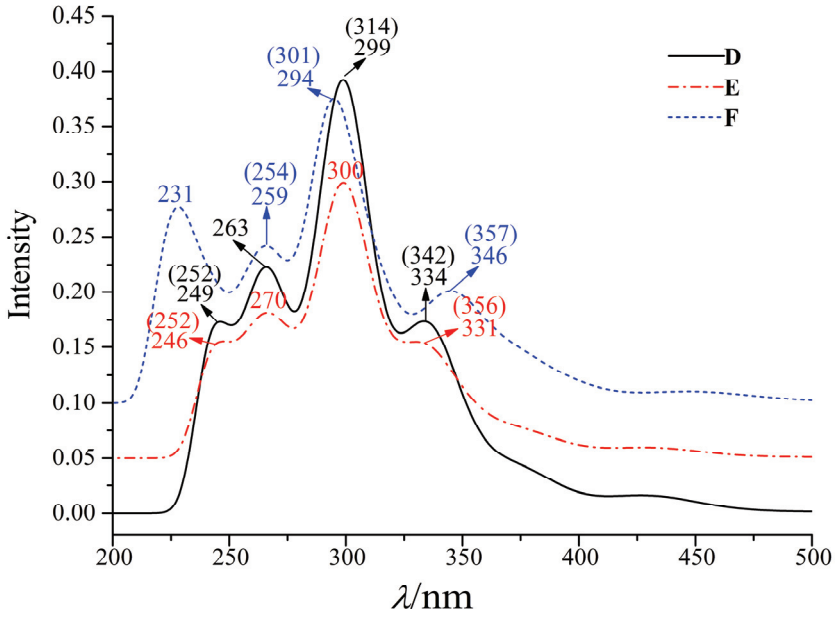

Fig. 7. Simulated absorption spectra (with Intensity as absorbance, *A*) in dichloromethane of complexes RuCO($AsPh_3$)L^2 (**D**), RuCO(PPh_3)L^2 (**E**) and RuCO(Py)L^2 (**F**) from the TD-B3LYP(PCM) calculations, together with the experimental values in parentheses.

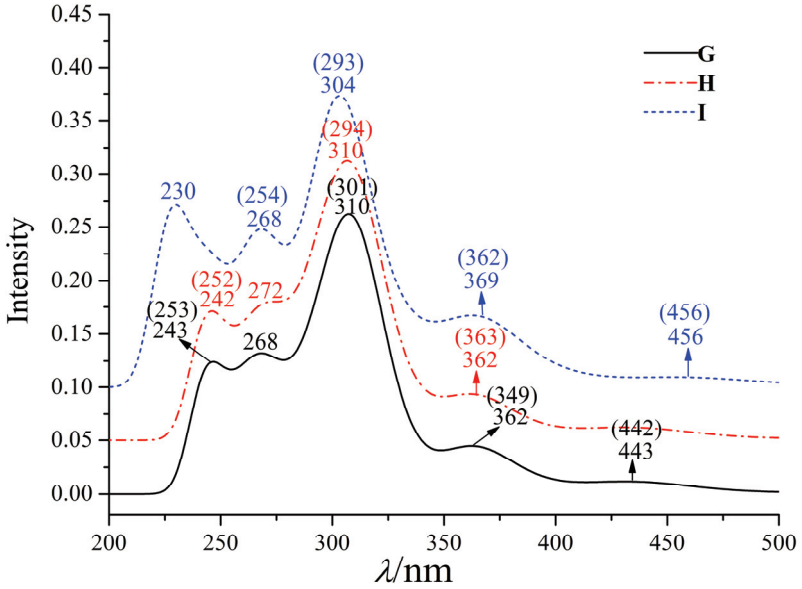

Fig. 8. Simulated absorption spectra (with Intensity as absorbance, *A*) in dichloromethane of complexes RuCO($AsPh_3$)L^3 (**G**), RuCO(PPh_3)L^3 (**H**) and RuCO(Py)L^3 (**I**) from the TD-B3LYP(PCM) calculations, together with the experimental values in parentheses.

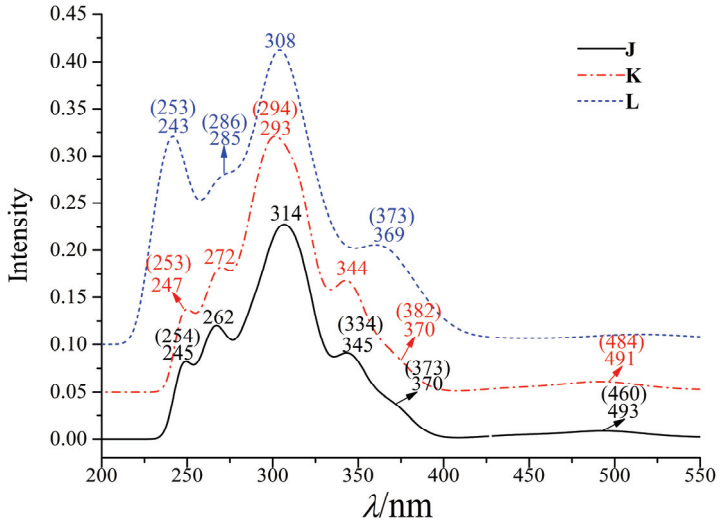

Fig. 9. Simulated absorption spectra (with Intensity as absorbance, *A*) in dichloromethane of complexes $RuCO(AsPh_3)L^4$ (**J**), $RuCO(PPh_3)L^4$ (**K**) and $RuCO(Py)L^4$ (**L**) from the TD-B3LYP(PCM) calculations, together with the experimental values in parentheses.

larger than the others, which shows an agreement with the experimental absorption intensity. Although the absolute values of the intensity between the theoretical and experimental results could not be compared, the relative sequence is consistent. If the peak intensity is considered as a dominant factor, the absorption band at 298 nm with the largest oscillator strength should correspond to the experiment peak at 258 nm. The deviation between them is as large as 0.65 eV, which is too large to be accepted. Furthermore, the theoretical absorption peaks of 294 nm for **C**, 301 nm for **F**, 293 nm for **I**, and 286 nm for **L** could not be related to any experimental absorption band. Therefore, the absorption peak position as the predominantly determined factor in this work is taken into account, which was usually adopted in previous literature.[35,36] For complexes **A**, the most intense absorption at 298 nm, dominantly associated with the transition from H-5 to L, is assigned as having a mixed intraligand charge-transfer (ILCT)/ligand–ligand charge-transfer (LLCT) character. The H-5 of complex **A** is dominantly composed of the π orbital of the Ph_1 and Ph_4 moieties, while the L presents the π* orbital character of Fu as well as the p orbital of the C_2 atom and the N atom in part a. Consequently, the transition related with the 298 absorption peak, which is not detected by experiment, is ascribed to a (p, π)→(p, π*) transition. The moderate absorption at 261 nm arises from the H-6→L+2 transition corresponding to a (π, d)→(p, d) transition with a mixed LL/ligand–metal charge-transfer (LMCT)/metal-center (MC) character. The other two weak absorptions at 331 and 444 nm originate respectively from H-4→L and H→L+1 transitions

with a mixed IL/metal–ligand (MLCT) character. In the experimental literature, the authors provide a tentative assignment that the band at 355–484 nm originates from the spin allowed $^1A_{1g}$ to $^1T_{1g}$ transition, which is not consistent with the theoretical result. To confirm the existence of d–d transitions, the distributions of the electron–hole of the S_4 and S_{14} states are plotted in Fig. S-7. It is clearly seen that the electrons are mainly extended over the Ph_1 (for the S_4 state)/Fu, C_2 and N_1 (for the S_{14} state), while the holes are predominantly localized at N_1, C_a and Ru (for the S_4 state) and Ph_1, O_1 and Ru (for the S_{14} state). Therefore, the transitions should be attributed to charge-transfer (CT) excitation rather than local excitation (LE). The distributions of the electron–hole for the other excited states of complex **A** are plotted in Fig. S-7. The detailed transition characters for the other complexes will not be discussed individually.

Discovering the common points among them is more crucial to provide essential guidance for further new complex design. One or two more absorption peaks failed to be measured experimentally were confirmed for all complexes. Moreover, some of them were main absorptions of high intensity, which testifies again that theoretical simulation is essential to elucidate and identify the spectroscopic properties. The second point is that the lowest-lying transition energies showed a complicated sequence, which does not obey the H–L energy gap. It is consistent with the expectation in the above section. However, some valuable clues could still be found for them. If the primary ligand is fixed, the lowest-lying absorption wavelengths decrease in the sequence of X = Py → $AsPh_3$ → PPh_3 with the exception of group *i*). If the second ligand is the same, complexes **J**, **K** and **L** with the $L^n = L^4$ have the largest lowest-lying singlet transition energy in the respective group and the corresponding wavelength will be blue-shifted. In summary, substituting the secondary ligand with Py ligand will decrease the lowest-lying transition energy, while the lowest-lying transition energy will increase with the improvement of the π-conjugation length of the primary ligand.

Based on the above data, no clear-cut sequence was obtained between the H–L energy gap and lowest-lying transition, which is mainly attributed to the relatively smaller lowest-lying absorption for complex **C**. The reasons for this exception could be an inaccurate prediction of the lowest-lying wavelength or of the H–L energy gap. To elucidate this puzzle, the HOMO energy, the LUMO energy, and H–L energy gap of complexes **A**, **B**, and **C** obtained at the B3LYP, M06, and PBE0 methods are listed in Table S-XV. The H–L energy gaps increased in the order of **C** < **A** < **B** with all three methods. In addition, the structures of complexes **A**, **B** and **C** were optimized by the B3LYP method with two different basis sets, 6-31G(d)-LANL2DZ and def2-SVP.[37,38] Similarly, the H–L energy gaps still changed in the same sequence and the largest deviation among them was only 0.02 eV at the def2-SVP level. Except for these DFT functionals and basis set, the absorption spectra of complexes **A**, **B** and **C** were also cal-

culated by the TD-CAM-B3LYP/def2-SVP method based on the structure optimized by various methods. There was no significant difference among the various methods (See Table S-XVI). Additionally, the detailed electronic transition properties in the absorption process calculated at TD-CAM-B3LYP/def2-SVP//B3LYP/6-31G(d)-LANL2DZ level are listed in Table S-XVII. Compared with the absorption features obtained at the TD-B3LYP/6-31G(d)-LANL2DZ//B3LYP/6-31G(d)-LANL2DZ level, the absorption band determined with the former functional showed a significant blue-shift. However, the transition characteristics of the corresponding excited states obtained by the two functionals give similar results. The lowest-lying absorption of complex **C** had the smallest absorption wavelength. The combination of primary ligand L^1 and secondary ligand Py did not lead to any change in the structure or spectrum. When the Py ligand was combined with the other three primary ligands, L^2–L^4, the lowest-lying absorption was red-shifted in the respective group. We hope that further experiments will be performed to provide more information to judge the effect of Py as the secondary ligand.

CONCLUSIONS

A series of ruthenium(II) thiosemicarbazone complexes [Ru(CO)(X)(L^n)] were investigated theoretically by the DFT and TDDFT methods. Detailed information about the electronic structures and absorption spectra was elucidated. The effect of the principal ligand (L^n) and the secondary ligand (X) was explored. Improving the π-conjugation of the end group increased the lowest-lying transition energy. The lowest-lying absorption wavelength was red-shifted using a Py group as the secondary ligand rather than an $AsPh_3$ or PPh_3 group.

SUPPLEMENTARY MATERIAL

Additional calculated data are available electronically from http://www.shd.org.rs/JSCS/, or from the corresponding author on request.

Acknowledgements. We thank the Beijing Key Laboratory of Ionic Liquids Clean Process and State Key Laboratory of Multiphase Complex Systems, Institute of Process Engineering, Chinese Academy of Sciences for providing the computational resources. This work was supported by the Natural Science Foundation of He'nan Province of China (144300510032 and 142300410120).

И З В О Д

ЕФЕКАТ ГЛАВНИХ И СЕКУНДАРНИХ ЛИГАНАДА НА ЕЛЕКТРОНСКЕ СТРУКТУРЕ И СПЕКТРЕ СЕРИЈЕ РУТЕНИЈУМ(II) КОМПЛЕКСА

YANLI ZHANG[1], JIEQIONG LI[2] и LI WANG[2]

[1]School of Materials and Chemical Engineering, Zhongyuan University of Technology, Zhongyuan 450007, P.R. China u [2]Institute of Environmental and Analytical Sciences, College of Chemistry and Chemical Engineering, Henan University, Kaifeng, Henan 475004, P.R. China

Урађено је истраживање помоћу DFT (теорија функционала густине, density functional theory)/TDDFT (теорија временски зависног функционала густине, time-dependent density functional theory) да би се проучиле геометрије основног стања, електронске структуре и апсорпциони спектри дванаест рутенијум(II) тиосемикарбазонских комплекса [Ru(CO)(X)(L^n)], где су L^n деривати двобазних тетрадентатних Шифових база као лиганада, а X $AsPh_3$/PPh_3/Py. Геометрије основних стања су оптимизоване на B3LYP/6-31G(d)-LANL2DZ нивоу, а спектри су симулирани помоћу TD-B3LYP/6-31G(d)--LANL2DZ методе на основу оптимизованих геометрија. Процењен је утицај примарних и секундарних лиганада (L^n и X) на карактер електронског прелаза и на положај апсорпционог максимума.

(Примљено 29. октобра 2015, ревидирано 15. јануара, прихваћено 17. фебруара 2016)

REFERENCES

1. R. N. Prabhu, D. Pandiarajan, R. Ramesh, *J. Organomet. Chem.* **694** (2009) 4170
2. M. Wang, L. F. Wang, Y. Z. Li, Q. X. Li, Z. D. Xu, D. M. Qu, *Transition Met. Chem.(Dordrecht, Neth.)* **26** (2001) 307
3. A. Chipeleme, J. Gut, P. J. Rosenthal, K. Chibale, *Bioorg. Med. Chem.* **15** (2007) 273
4. T. Rosu, A. Gulea, A. Nicolae, R. Georgescu, *Molecules* **12** (2007) 782
5. A. Panja, C. Campana, C. Leavitt, M. J. Van Stipdonk, D. M. Eichhorn, *Inorg. Chim. Acta* **362** (2009) 1348
6. V. V. Bon, S. I. Orysyk, V. I. Pekhnyo, S. V. Volkov, *J. Mol. Struct.* **984** (2010) 15
7. M. X. Li, D. Zhang, L. Z. Zhang, J. Y. Niu, B. S. Ji, *J. Organomet. Chem.* **696** (2011) 852
8. B. D. Clercq, F. Verpoort, *Macromolecules* **35** (2002) 8943
9. T. Opstal, F. Verpoort, *Synlett* **6** (2002) 935
10. T. Opstal, F. Verpoort, *Angew. Chem. Int. Ed.* **42** (2003) 2876
11. T. E. Keyes, B. Evrard, J. G. Vos, C. Brady, J. J. McGarvey, P. Yayaweera, *Dalton Trans.* **15** (2004) 2341
12. E. M. Kober, J. Carper, R. S. Lumpkin, T. J. Meyar, *J. Phys. Chem.* **90** (1986) 3722
13. M. Muthukumar, P. Viswanathamurthi, *J. Coord. Chem.* **63** (2010) 1263
14. S. Kannan, M. Sivagamasundari, R. Ramesh, Y. Liu, *J. Organomet. Chem.* **693** (2008) 2251
15. V. Mahalingam, N. Chitrapriya, F. R. Fronczek, K. Natarajan, *Polyhedron* **27** (2008) 2743
16. M. U. Raja, N. Gowri, R. Ramesh, *Polyhedron* **29** (2010) 1175
17. G. Raja, N. Sathya, C. Jayabalakrishnan, *J. Coord. Chem.* **64** (2011) 817
18. Gaussian 09, Revision A.02, Gaussian, Inc., Wallingford, CT, 2009
19. A. D. Becke, *J. Chem. Phys.* **98** (1993) 5648
20. C. Lee, W. Yang, R. G. Parr, *Phys. Rev. B* **37** (1988) 785
21. P. J. Stephens, F. J. Devlin, C. F. Chabalowski, M. J. Frich, *J. Phys. Chem.* **98** (1994) 11623

22. J. P. Perdew, K. Burke, M. Ernzerhof, *Phys. Rev. Lett.* **77** (1996) 3865
23. Y. Zhao, D. G. Truhlar, *Theor. Chem. Acc.* **120** (2008) 215
24. K. Saito, Y. Nakao, S. Sakaki, *Inorg. Chem.* **47** (2008) 4329
25. W. J. Hehre, R. Ditchfield, J. A. Pople, *J. Chem. Phys.* **56** (1972) 2257
26. W. R. Wadt, P. J. Hay, *J. Chem. Phys.* **82** (1985) 284
27. W. R. Wadt, P. J. Hay, *J. Chem. Phys.* **82** (1985) 299
28. W. R. Wadt, P. J. Hay, *J. Chem. Phys.* **82** (1985) 270
29. R. Bauernschmitt, R. Ahlrichs, *Chem. Phys. Lett.* **256** (1996) 454
30. M. E. Casida, C. Jamorski, K. C. Casida, D. R. Salahub, *J. Phys. Chem.* **108** (1998) 4439
31. R. E. Stratmann, G. E. Scuseria, M. J. Frisch, *J. Chem. Phys.* **109** (1998) 8218
32. Š. Miertus, E. Scrocco, J. Tomasi, *Chem. Phys.* **55** (1981) 117
33. J. Tomasi, M. Persico, *Chem. Rev.* **94** (1994) 2027
34. D. Pandiarajan, R. Ramesh, *Inorg. Chem. Commun.* **14** (2011) 686
35. R. Heydová, E. Gindensperger, R. Romano, J. Sýkora, A. Vlček, Jr., S. Zaĺis, C. Daniel, *J. Phys. Chem., A* **116** (2012) 11319
36. D. Jacquemin, E. A. Perpète, I. Ciofini, C. Adamo, *Theor. Chem. Acc.* **120** (2008) 405
37. F. Weigend, R. Ahlrichs, *Phys. Chem. Chem. Phys.* **7** (2005) 3297
38. D. Andrae, U. Haeussermann, M. Dolg, H. Stoll, H. Preuss, *Theor. Chim. Acta* **77** (1990) 123.